



Since January 2020 Elsevier has created a COVID-19 resource centre with free information in English and Mandarin on the novel coronavirus COVID-19. The COVID-19 resource centre is hosted on Elsevier Connect, the company's public news and information website.

Elsevier hereby grants permission to make all its COVID-19-related research that is available on the COVID-19 resource centre - including this research content - immediately available in PubMed Central and other publicly funded repositories, such as the WHO COVID database with rights for unrestricted research re-use and analyses in any form or by any means with acknowledgement of the original source. These permissions are granted for free by Elsevier for as long as the COVID-19 resource centre remains active.

Identification of Nucleocapsid Binding Sites within Coronavirus-Defective Genomes

Raymond Cologna,¹ Jeannie F. Spagnolo, and Brenda G. Hogue²

Department of Molecular Virology and Microbiology, Baylor College of Medicine, Houston, Texas 77030

Received February 23, 2000; returned to author for revision March 31, 2000; accepted August 24, 2000

The coronavirus nucleocapsid (N) protein is a major structural component of virions that associates with the genomic RNA to form a helical nucleocapsid. N appears to be a multifunctional protein since data also suggest that the protein may be involved in viral RNA replication and translation. All of these functions presumably involve interactions between N and viral RNAs. As a step toward understanding how N interacts with viral RNAs, we mapped high-efficiency N-binding sites within BCV- and MHV-defective genomes. Both *in vivo* and *in vitro* assays were used to study binding of BCV and MHV N proteins to viral and nonviral RNAs. N-viral RNA complexes were detected in bovine coronavirus (BCV)-infected cells and in cells transiently expressing the N protein. Filter binding was used to map N-binding sites within Drep, a BCV-defective genome that is replicated and packaged in the presence of helper virus. One high-efficiency N-binding site was identified between nucleotides 1441 and 1875 at the 3' end of the N ORF within Drep. For comparative purposes N-binding sites were also mapped for the mouse hepatitis coronavirus (MHV)-defective interfering (DI) RNA MIDI-C. Binding efficiencies similar to those for Drep were measured for RNA transcripts of a region encompassing the MHV packaging signal (nts 3949–4524), as well as a region at the 3' end of the MHV N ORF (nts 4837–5197) within MIDI-C. Binding to the full-length MIDI-C transcript (~5500 nts) and to an ~1-kb transcript from the gene 1a region (nts 935–1986) of MIDI-C that excluded the packaging signal were both significantly higher than that measured for the smaller transcripts. This is the first identification of N-binding sequences for BCV. It is also the first report to demonstrate that N interacts *in vitro* with sequences other than the packaging signal and leader within the MHV genome. The data clearly demonstrate that N binds coronavirus RNAs more efficiently than nonviral RNAs. The results have implications with regard to the multifunctional role of N. © 2000 Academic Press

INTRODUCTION

The coronavirus genome is a single-stranded, positive-sense, 27- to 32-kb RNA molecule, the largest among all RNA viruses. The genomic RNA is encapsidated by multiple copies of the nucleocapsid (N) protein and is packaged as a helical nucleocapsid in the mature enveloped virion (Kennedy and Johnson-Lussenburg, 1975; Macneughton and Davies, 1978; Caul *et al.*, 1979; Davies *et al.*, 1981). Recently it was suggested that coronaviruses contain a more structured, possibly icosahedral, core consisting of the membrane (M) and N proteins surrounding a helical nucleocapsid (Risco *et al.*, 1996).

All coronavirus N proteins are 50- to 60-kDa phosphoproteins, with an overall high basic amino acid content. Within any antigenic subgroup the amino acid sequence homology is high, whereas the proteins are highly divergent across the different antigenic subgroups (Lapps *et al.*, 1987). Three structural domains are present in the N protein (Parker and Masters, 1990). The middle domain is

responsible for RNA binding (Masters, 1992; Nelson and Stohlgman, 1993; Nelson *et al.*, 2000). During a normal infection, N is one of the most abundantly expressed viral proteins, expressed at a much higher level than any of the viral replication factors that are expected to interact with viral RNAs.

Other functions, in addition to its known structural role, have been postulated for N. Data suggest that N may be involved in viral transcription (Compton *et al.*, 1987; Baric *et al.*, 1988) and translation control (Tahara *et al.*, 1994). MHV N colocalizes with putative replicase proteins in virus-infected cells, providing further support that N may be involved in RNA replication (van der Meer *et al.*, 1999; Denison *et al.*, 1999). It was recently demonstrated that N interacts with heterogeneous nuclear ribonucleoprotein A1 (hnRNP-A1), both *in vitro* and *in vivo* (Wang and Zhang, 1999). Cellular hnRNP-A1 binds to MHV negative-strand leader and intergenic sequences (Li *et al.*, 1997). It has been postulated that hnRNP plays a role in MHV transcription (Zhang and Lai, 1995).

In this study we analyzed N-RNA interactions to begin addressing the mechanism by which N recognizes viral RNAs. Multiple assays were used to gain insight into N-RNA interactions that may be involved in coronavirus RNA packaging, nucleocapsid assembly, and other postulated functions of N. Quantitative analysis of N-RNA interactions revealed that N interacts more efficiently

¹ Present address: Southwestern Foundation for Biomedical Research, Department of Virology and Immunology, San Antonio, TX 78227.

² To whom correspondence and reprint requests should be addressed at Baylor College of Medicine, Department of Molecular Virology and Microbiology, One Baylor Plaza, Houston, TX 77030. Fax: (713) 798-7375. E-mail: bhogue@bcm.tmc.edu.

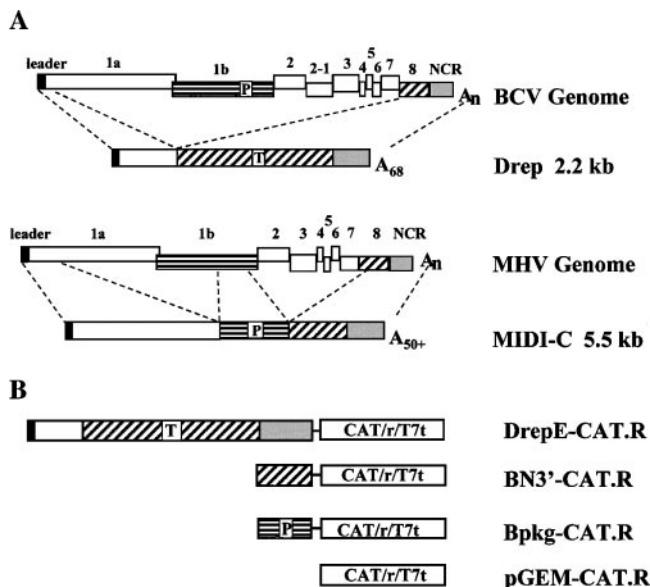


FIG. 1. Schematic of two coronavirus-defective genomes and chimeric RNAs used to test the ability of the high-efficiency N-binding site to function as a packaging signal. (A) Drep is a cloned BCV-defective RNA (Chang *et al.*, 1994) and pMIDI-C is a cloned MHV-A59 DI (van der Most *et al.*, 1991). The various parts of the genome that are included in each defective genome are labeled. Drep includes a 30-nt reporter sequence (T) derived from the TGEV N gene (Chang *et al.*, 1994). The approximate position of the packaging signal (P) within the BCV and MHV genomes, as well as MIDI-C, is indicated. (B) Chimeric RNAs were made from coronavirus sequences (Drep, BCVN3', and BCVpkg) cloned at the 5' end of a cassette that contains the CAT gene, the hepatitis delta virus ribozyme (r), and the T7 terminator (T7t).

with coronavirus RNA than with noncoronavirus RNA. High-efficiency binding regions were mapped for the BCV-defective genome RNA Drep and defective interfering (DI) MHV RNA MIDI-C (de Groot *et al.*, 1992; Chang *et al.*, 1994) (Fig. 1). Both defective genomes are replicated and packaged by their parental virus. BCV and MHV belong to the same antigenic subgroup. Sequence comparisons indicate that the two viruses are closely related (Lapps *et al.*, 1987; Abraham *et al.*, 1990a,b; Kienzle *et al.*, 1990). Even though the two viruses share many similarities, they appear to differ with regard to RNA packaging. BCV packages subgenomic RNA in addition to genomic RNA (Hofmann *et al.*, 1990), whereas MHV packages very little, if any, of its subgenomics. BCV Drep is replicated and packaged by BCV, but it does not contain any gene 1b sequence (Fig. 1) (Chang *et al.*, 1994; Cologna and Hogue, 2000). MIDI-C contains part of gene 1b where a packaging signal maps (van der Most *et al.*, 1991; Fosmire *et al.*, 1992) (Fig. 1). We recently identified a packaging signal in the BCV genome that is homologous to the MHV packaging signal (Cologna and Hogue, 2000). Our analyses of N-binding sites within the BCV and MHV defective genomes provide the most comprehensive and comparative study to date of coronavirus N-RNA interactions.

RESULTS

BCV N-RNA complexes are present in virus-infected cells

When we began our investigation to understand how coronavirus RNAs are recognized by the N protein, our main focus was directed at the identification of a packaging signal for the bovine coronavirus-defective RNA Drep (Chang *et al.*, 1994). We hypothesized at the time, based on data from other studies in our lab, that Drep might contain a packaging signal within its N open reading frame (ORF).

Identification of a packaging signal within Drep by deletion mapping was not possible because of technical limitations. Drep replication is readily compromised by only small deletions or point mutations (Chang and Brian, 1996; Cologna and Hogue, unpublished data). Therefore, toward our goal to identify a packaging signal for Drep, we initially assayed for N-viral RNA interactions using four different approaches. The rationale was that identification of N-binding sites on the Drep RNA could give us insight toward what interactions are important for Drep packaging.

We first determined which viral RNAs interact with N during a BCV infection. Mock- and BCV-infected HCT cells were metabolically labeled with [³²P]orthophosphate in the absence of actinomycin D. Both viral and cellular RNAs are labeled in the absence of the inhibitor, whereas only viral RNAs are labeled in the presence of the inhibitor. Cytoplasmic RNAs were either examined directly or after immunoprecipitation with antibodies specific for the N protein. Antibodies against the spike protein (S) or preimmune sera were used as controls. As expected, in the absence of actinomycin D a large amount of label was incorporated into ribosomal RNAs (Fig. 2A, lanes 1 and 2). Weaker viral RNA signals were observed over the background when total RNA from infected cells was analyzed directly (Fig. 2A, lane 2). Genomic and subgenomic RNAs were clearly visible from BCV-infected cells labeled in the presence of actinomycin D, whereas no RNAs were seen with mock-infected cells (Fig. 2A, lanes 3 and 4). A profile typical of virus genomic and subgenomic RNAs was observed for RNAs coimmunoprecipitated with antibodies against N (Fig. 2A, lanes 5 and 6). Immunoprecipitation with the BCV S-specific antibodies demonstrated that the N-RNA complexes were specific for the N protein and that we were not merely recovering translation complexes. In all experiments, specific immunoprecipitation of the N and S proteins was verified by SDS-PAGE/Western blotting analysis (data not shown).

The coprecipitated RNAs from cells labeled in the absence of actinomycin D comigrated with viral RNAs that were labeled and analyzed directly from cells labeled in the presence of actinomycin D (Fig. 2A,

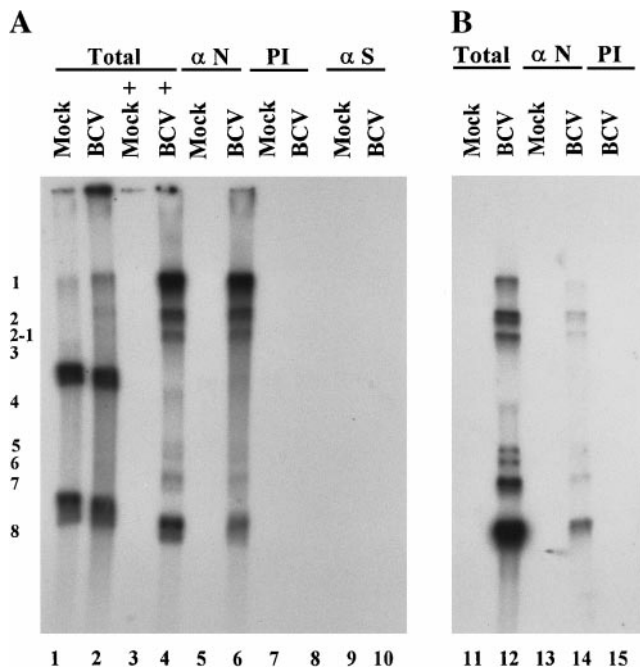


FIG. 2. Metabolic labeling and Northern blot analyses of BCV specific N-RNA complexes. (A) HCT cells were infected with BCV or mock-infected. Viral RNAs were labeled with [32 P]orthophosphate in the presence (lanes 3 and 4) or absence (lanes 1 and 2, 5–10) of actinomycin D. RNAs were analyzed directly (lanes 1–4) or after immunoprecipitation (lanes 5–10). Protein-RNA complexes were immunoprecipitated with anti-N (lanes 5 and 6) polyclonal antibodies, the preimmune serum (lanes 7 and 8) or anti-S ascites (lanes 9 and 10). (B) Unlabeled RNAs were isolated and run in parallel. Viral RNAs from total cytoplasmic RNA (lanes 11 and 12) and immunocomplexes using the anti-N (lanes 13 and 14) polyclonal antibodies and the preimmune serum (lane 15) were detected with a [32 P]-labeled N gene-specific riboprobe.

compare lanes 4 and 6). No RNAs were recovered using control sera (Fig. 2A, lanes 7–10). Therefore, the coimmunoprecipitated RNAs were assumed to be viral RNAs. To support this assumption, unlabeled N-RNA complexes were isolated and Northern blots were probed with a BCV N ORF-specific probe that recognizes genomic and all subgenomic RNAs. Genomic and subgenomic RNAs were readily detected in the total RNA fractions (Fig. 2B, lane 12) and in the N-RNA complexes isolated by immunoprecipitation from the same lysate (Fig. 2B, lane 14), but not from mock-infected cell lysates (Fig. 2B, lanes 11 and 13). No RNAs were coimmunoprecipitated with preimmune serum (Fig. 2B, lane 15).

These results demonstrated for the first time that N interacts with all viral RNAs during a BCV infection. Since N-RNA complexes were isolated from cells labeled in the absence of actinomycin D, the results suggest that the N-viral RNA interactions are specific. Although we cannot rule out the possibility that weakly labeled cellular RNAs comigrated with the viral RNAs, no prominently labeled cellular RNAs appeared to be associated with N.

BCV N binds coronavirus RNA more efficiently than noncoronavirus RNA

An in-solution binding assay (Geigenmuller-Gnirke *et al.*, 1993) was used as a second approach to analyze N-RNA interactions and further address the question of specificity. In this assay *in vitro* generated, unlabeled N and Drep RNA transcripts were incubated with *in vitro* translated [35 S]methionine-labeled BCV N protein. Protein-RNA interactions were measured by comigration of [35 S]-labeled N protein with unlabeled RNA. When no RNA was included in the reaction mix, N protein did not enter the agarose gel (Fig. 3, lane 1). A twofold molar excess of total cytoplasmic BHK RNA was included as a competitor in reactions (Fig. 3, lanes 2–7). N protein interacted weakly with both 18S and 28S ribosomal RNAs when only BHK RNA was included in reactions (Fig. 3, lane 2). However, when coronavirus-specific transcripts Drep and N were included, N protein appeared to preferentially bind the coronavirus RNAs over the ribosomal RNA (Fig. 3, compare lanes 2–4).

Influenza virus neuraminidase (NA) gene transcripts were also examined to further assess what appeared to be preferential binding to coronavirus RNA. The full-length transcript is comparable in size and nucleotide content to the BCV N gene. N protein did bind NA transcript (Fig. 3, lane 7). Since the signal was distorted by comigration of full-length NA RNA with 18S ribosomal RNA, shorter NA transcripts were examined to more clearly assess N-binding to the NA RNA (Fig. 3, lanes 5 and 6). Binding to the NA RNA was less than half of that

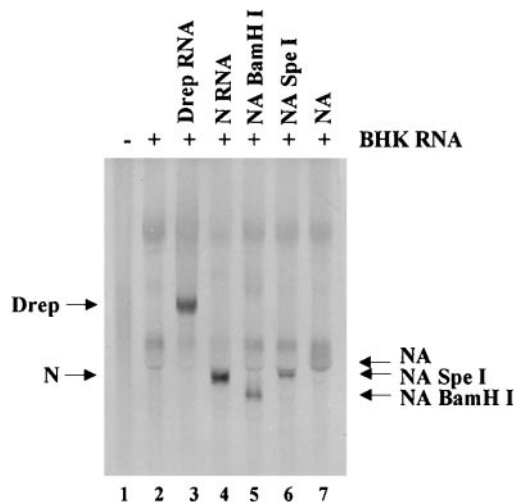


FIG. 3. Detection of BCV N-RNA interactions by an in-solution binding assay. A 1- μ g sample of unlabeled Drep (lane 3) and equal molar amounts of each of the other RNAs (N [lane 4], NA BamHI [lane 5], NA Spe1 [lane 6], and full-length NA [lane 7]) were incubated with *in vitro* translated, [35 S]-labeled BCV N protein. RNAs are visualized by the comigration of the labeled N protein with unlabeled RNAs (lanes 3–7). A 5- μ g sample (\sim 2.2 M excess) of BHK total cytoplasmic RNA were included as a competitor in all reactions (lanes 2–7), except the reaction containing no RNA (lane 1).

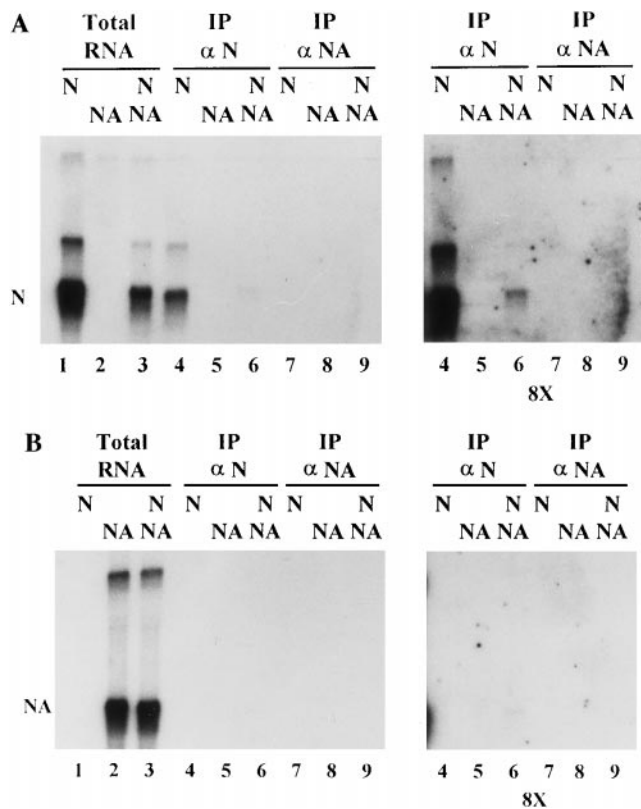


FIG. 4. Isolation of N-RNA complexes from cells transiently expressing BCV N. vTF7-3-infected BHK cells were transfected with plasmids containing a cDNA copy of the N gene (pN.R1.1), the influenza NA gene (pNA.R1), or cotransfected with both plasmids. RNAs were divided in half and run on parallel denaturing agarose gels for Northern blotting using equal amounts of either a BCV N gene-specific riboprobe (A) or an influenza NA gene-specific riboprobe (B). Total cytoplasmic RNA from transfected cells was analyzed directly (lanes 1–3) or after immunoprecipitation with anti-N (lanes 4–6) or anti-NA (lanes 7–9) polyclonal sera. Right panels (lanes 4–9) were exposed eight times longer than the left panels.

measured for a comparable molar amount of N RNA (Fig. 3, lanes 3–6). The results provided further direct data that N interacts with coronavirus RNAs and suggested that the protein binds viral RNAs more efficiently than non-coronavirus RNAs.

To determine whether BCV N protein interacts with the N gene when expressed in the absence of a coronavirus infection, a third approach was used. BCV N and influenza virus NA genes were expressed using vTF7-3, the vaccinia virus recombinant that expresses T7 RNA polymerase (Fuerst *et al.*, 1986). Following infection with vTF7-3, BHK cells were transfected with plasmids that contained the BCV N gene or the influenza virus NA gene, singly and together (Fig. 4). At 16 h posttransfection cytoplasmic RNAs were analyzed either directly (Figs. 4A and 4B, lanes 1–3) or after immunoprecipitation with purified N-specific antibodies (Figs. 4A and 4B, lanes 4–6) or antibodies against NA (Figs. 4A and 4B, lanes 7–9). RNAs were run on parallel agarose gels and

analyzed by Northern blotting using BCV N-specific (Fig. 4A) or NA-specific (Fig. 4B) 32 P-labeled riboprobes.

N-specific transcripts were present in cells transfected with the N gene plasmid (Fig. 4A, lanes 1 and 3), but not in vTF7-3-infected cells transfected with only the NA gene plasmid (Fig. 4A, lane 2). N-RNA complexes were coimmunoprecipitated from cells transfected with the N plasmid alone (Fig. 4A, lane 4) and from cells cotransfected with both N and NA plasmids (Fig. 4A, lane 6, 8X exposure). No N transcripts were coprecipitated when only the NA gene was expressed (Fig. 4A, lane 5). The amount of N transcripts from cells transfected with only the N gene was always higher than when the N and NA plasmids were coexpressed. Transfection optimization experiments did not correct the disparity, which may explain in part the reason for the significant decrease in the amount of N-N RNA complexes that were recovered in the presence of NA RNA expression.

Using the NA gene-specific riboprobe NA transcripts were detected when the NA plasmid was transfected alone or in combination with N plasmid, but not when the latter was transfected alone (Fig. 4B, lanes 1–3). No N-NA RNA complexes were immunoprecipitated with antibodies against the NA protein (Fig. 4B, lanes 7–9), again indicating that our buffer conditions disrupted translation complexes. However, a very small amount of NA-RNA complex was detected when the coexpressed N and NA genes were immunoprecipitated with the N antibodies (Fig. 4B, lane 6, 8X exposure).

The results were consistent with those from the insolubilization experiments. Absolute specificity of N-viral RNA interactions was not observed. However, N interacted more efficiently with its own ORF.

To determine whether the N protein interacts *in trans* with Drep RNA, we coexpressed both using the vaccinia T7 expression system as described above. Drep RNA expressed alone was immunoprecipitated with antibodies against N (data not shown). Drep contains an ORF consisting of a fusion between the amino-terminal portion of gene 1a and the entire N ORF (Chang *et al.*, 1994). The N portion of the Pol-N fusion protein apparently retains its RNA-binding function since Drep RNA-containing complexes were immunoprecipitated with N antibodies. The Pol-N fusion ORF is translated *in vitro* and immunoprecipitated with N-specific antibodies (Chang and Brian, 1996); therefore, expression of the Pol-N fusion protein made it impossible to definitively demonstrate interactions between N and Drep with this assay.

Mapping N-binding sites by filter binding

After establishing that N appeared to interact better with its viral RNAs than with noncoronavirus RNAs, we developed a nitrocellulose filter-binding assay to map and characterize the interactions of N with viral-specific RNA in a quantitative manner. This assay also allowed

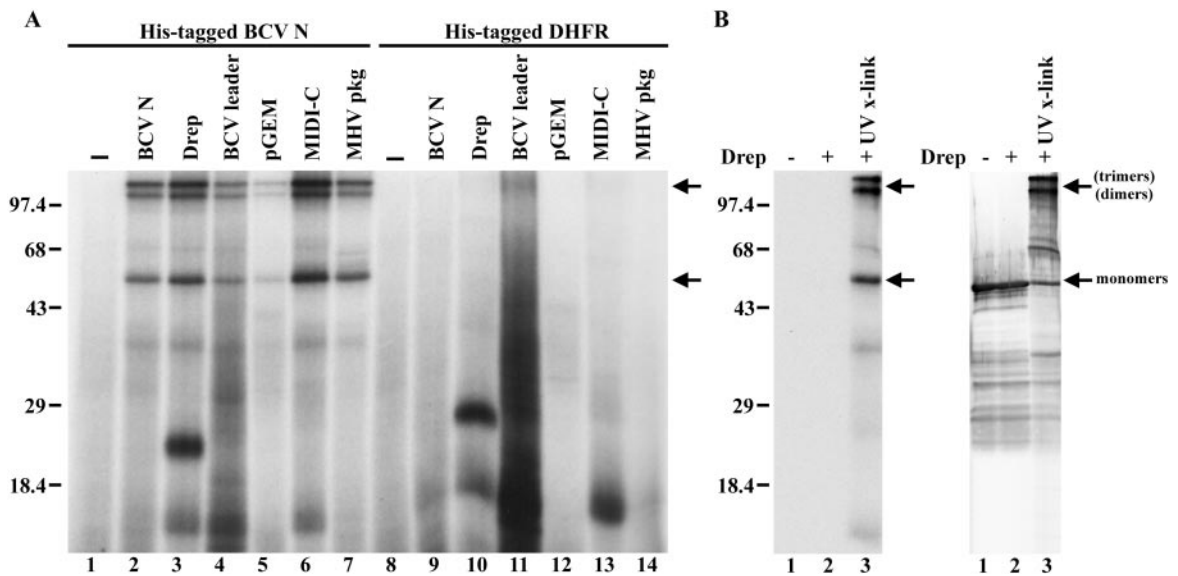


FIG. 5. UV crosslinking/Western blotting of purified his-BCV N to RNA. (A) [32 P]-labeled RNA probes, as indicated above each lane, were incubated with purified, bacterially expressed his-tagged BCV N protein (lanes 2–7) or DHFR protein (lanes 9–14) as described for filter-binding reactions, followed by UV crosslinking, RNase treatment, and SDS–PAGE. Probes in lanes 1 and 8 were incubated in the absence of protein. (B) His-tagged BCV N protein was incubated in the absence (lane 1, both panels) or presence of [32 P]-labeled Drep RNA (lanes 2 and 3, both panels) as described for filter-binding reactions. Half of each reaction that contained labeled probe was UV crosslinked (lane 3, both panels). Following SDS–PAGE the gel was blotted onto nitrocellulose and the membrane was analyzed directly by autoradiography (left panel) and by Western blotting using N-specific antibodies (right panel).

us to look more closely at specificity. The reaction conditions were initially established using purified histidine (his)-tagged BCV N protein that had been expressed in bacteria. We previously reported our preliminary results using the his-tagged N, which demonstrated that N binds Drep, MHV DI MIDI-C, and a transcript that contained the MHV packaging signal more efficiently than a noncoronavirus RNA (Cologna and Hogue, 1998).

To directly demonstrate that the his-tagged N protein was binding to the Drep, MIDI-C, and MHV packaging signal RNAs, UV crosslinking was performed following incubation of filter-binding reactions. After RNase A digestion covalently crosslinked proteins were analyzed by SDS–PAGE. A protein corresponding to the expected molecular mass of ~50 kDa for N crosslinked to equivalent molar amounts of all the coronavirus RNAs, including a 266-nt leader-containing RNA from the 5' end of the BCV genome (Fig. 5A, lower arrow, lanes 2–7). Two slower migrating species were also strongly crosslinked to the RNAs (Fig. 5A, upper arrow, lanes 2–7). Protein species of the same size also crosslinked to the control pGEM RNA (Fig. 5A, lane 5). However, less protein bound the pGEM RNA than the coronavirus-specific RNA transcripts, consistent with the earlier preliminary filter-binding results, suggesting that N binds coronavirus RNAs better than it binds heterologous RNAs (Cologna and Hogue, 1998).

Western blotting was used to confirm that the slower-migrating species that crosslinked to the RNAs were indeed his-BCV N. Filter-binding/UV crosslinking reac-

tions were assembled with 32 P-labeled Drep RNA and his-tagged BCV N protein. After SDS–PAGE, gels were blotted to nitrocellulose and analyzed by Western blotting using N-specific antibodies, followed by autoradiography (Fig. 5B, right and left panels, respectively). The slower-migrating ~50-kDa crosslinked species and the slowest-migrating higher-molecular-weight species (Fig. 5B, left panel, lane 3, arrows) were identified as N by Western blotting, thus directly confirming that N binds Drep RNA (Fig. 5B, right panel, lanes 1–3, arrows). The sizes of the slower-migrating forms correspond to those expected for dimer and trimer forms of N.

As a control, bacterially expressed his-tagged dihydrofolate reductase (DHFR) was purified in parallel with his-tagged BCV N and also used in the filter-binding/UV crosslinking assay. This control clearly demonstrated that no proteins in the molecular weight range of N crosslinked to the RNAs (Fig. 5A, lanes 8–14). However, the results also indicated that a bacterial contaminant with an apparent molecular weight of ~15 kDa crosslinked to some of the RNAs (Fig. 5, lower band in lanes 3, 4, 6, 10, and 13). The contaminant was present in the purified preparation of both his-BCV N and the DHFR control protein, even though both appeared to be more than 90% pure (data not shown). The heavily labeled band that migrated above the bacterial contaminant in lanes 3 and 10 of Fig. 5 is an RNase-resistant structure that was consistently observed with the Drep probe.

Attempts to obtain purified his-tagged N protein preparations that lacked the bacterial contaminant were not

successful. In addition to the copurification of the bacterial protein, we also had other concerns about the bacterially expressed protein. The tagged N had been purified under denaturing conditions, and even though the protein had been renatured, this raised concerns that the protein might not be refolding into its native form. Also, the protein was not phosphorylated when expressed in bacteria (data not shown). The role of phosphorylation is not known at this time; however, N is phosphorylated in virus-infected cells and in virions. To circumvent these problems, we chose to use infected cell lysates as the source of N protein for the completion of our study.

Filter-binding reactions were initially set up using Drep and pGEM RNA transcripts and both mock-infected and BCV-infected HCT cell lysates. Filter-binding reactions were assembled in double the normal volume. After incubation half of each reaction was removed and applied directly to nitrocellulose filters. Filters were washed and the amount of bound RNA was determined. The other half of each reaction was immunoprecipitated with N-specific polyclonal antibodies to recover N–RNA complexes. This provided a measurement of the extent to which N was associated with the RNAs that were detected by direct filter binding.

Almost 60% of Drep RNA transcripts were retained on filters after incubation with infected cell lysate, compared with about 15% of the RNA that was incubated with mock-infected lysate (Fig. 6A, Direct). Roughly 35% of the Drep-infected lysate complexes were immunoprecipitated with N-specific antibodies (Fig. 6A, IP). Therefore, more than 60% of the Drep RNA that was retained by direct filter binding was recoverable by immunoprecipitation. The amount of pGEM RNA retained by direct filter binding with either lysate was similar to the amount of Drep RNA retained by the binding of mock-infected cellular proteins (Fig. 6A, Direct). Only background levels (2–5%) of Drep RNA–protein complexes with mock-infected lysate and pGEM RNA–protein complexes with either lysate were immunoprecipitated with N-specific antibodies (Fig. 6A, IP). These data demonstrated that proteins in infected cell lysates bound the coronavirus RNA better than they bound noncoronavirus RNAs. The results clearly showed that the viral N protein was stably associated with the majority of these RNA–protein complexes.

We also directly visualized N-binding to Drep RNA. UV crosslinking and Western blotting were performed following incubation of filter-binding reactions. N in BCV-infected cell lysates, but not from mock-infected cells, clearly bound Drep transcripts (Fig. 7A, lanes 2 and 3).

From our data we cannot absolutely rule out the possibility that other viral proteins also bound Drep RNA and contributed to the increased filter binding with infected cell lysates. From the UV crosslinking results none of the major structural proteins (S, HE, or M) appeared to bind Drep. We expect that some of the viral replicase proteins

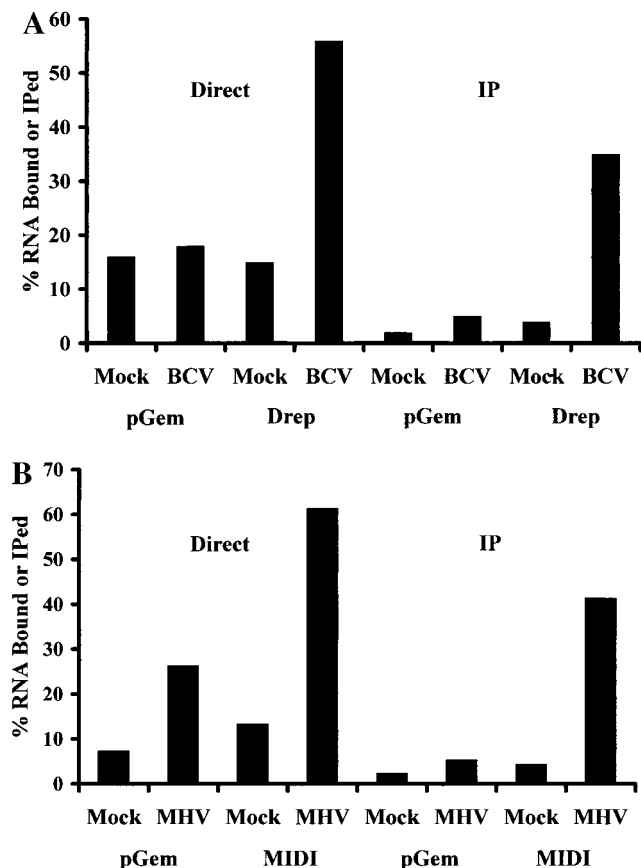


FIG. 6. Complex formation between N protein and defective genome RNAs of BCV and MHV. Complexes between infected and mock-infected lysate proteins and defective genome RNAs were detected by filter binding. pGEM transcripts were analyzed in parallel as controls. (A) Drep RNA was incubated with BCV-infected or mock-infected HCT lysates. (B) MHV MIDI-C RNA was incubated with MHV-infected or mock-infected 17C11 cell lysates. Half of each binding reaction was filtered through nitrocellulose membranes and Cerenkov counted (A and B, four left columns, Direct). The other half of each reaction was immunoprecipitated with N-specific antibodies. Immunoprecipitated N–RNA complexes were recovered with protein A–Sepharose and counted (A and B, four right columns, IP). The data represent the means of two and three experiments for MHV and BCV, respectively.

might also bind regions of the RNA that are involved in RNA replication. However, these proteins are far less abundant than the N protein and most likely would not be detected by UV crosslinking.

To determine whether specific N-binding sites are present within Drep, a series of transcripts were designed to map sequences within the RNA that interact with N. The maximum binding efficiency was measured for each transcript by filter binding (Table 1). Maximum N-binding efficiency was defined as the percentage of RNA that was retained on the filter, compared to the total amount of labeled RNA added to the reaction. Terminal sequences, including the leader, Pol5', and BCV3'NCR were bound much less efficiently than was full-length Drep. The binding efficiencies for these transcripts were similar to the nonviral RNAs pGEM and CAT. Transcripts

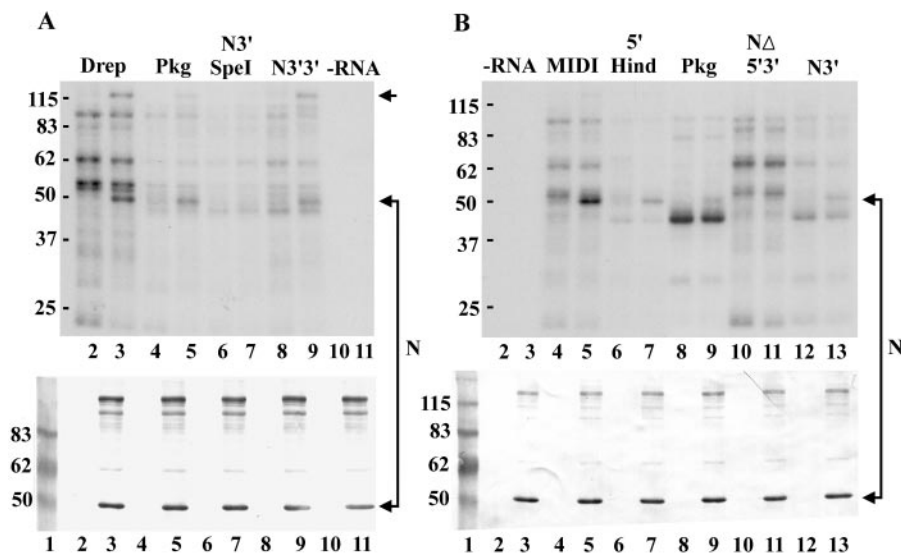


FIG. 7. UV crosslinking/Western blotting of N from infected cell lysates to RNAs. (A) [32 P]-labeled BCV RNA transcripts, as indicated above each lane, were incubated with either BCV-infected (odd-numbered lanes) or mock-infected (even-numbered lanes) HCT cell lysates as described for filter-binding reactions, followed by UV crosslinking, RNase treatment, and SDS-PAGE. After SDS-PAGE gels were blotted onto nitrocellulose. Membranes were analyzed directly by autoradiography (upper panel) and by Western blotting using N-specific antibodies (lower panel). Cell lysates were incubated in the absence of labeled probe in lanes 10 and 11. All probes were incubated in the absence of protein and analyzed on a parallel gel as a control for each reaction (data not shown). (B) [32 P]-labeled MHV transcripts were incubated with MHV-infected (odd-numbered lanes) or mock-infected 17C11 cells (even-numbered lanes) and analyzed as described above. Lysates in lanes 2 and 3 were not incubated with probe. Connected arrows indicate the position of crosslinked N (upper panels) and corresponding position detected by Western blotting (lower panels). The single arrow in (A) notes the position of oligomeric N. The positions of molecular weight standards are indicated at the left of each panel.

N, N3', and N3'3', all from within the N ORF, were bound at efficiencies ranging from 57 to 73%. These binding efficiencies were comparable to measurements for full-

length Drep. Other transcripts, N5' and N3' SpeI, also from within the N ORF, were bound less efficiently at 22 and 12%, respectively. Only low-level binding was ob-

TABLE 1

Maximum BCV N Binding Efficiencies for Drep and Related RNAs

Transcript	Schematic	Size (nt)	Maximum N binding efficiency ^a
Drep		2231	62.7 ± 1.9
leader		266	12.1 ± 9.2
Pol5'		422	9.5 ± 0.7
BCV3'NCR		354	20.0 ± 7.9
BCV1b		303	37.2 ± 1.9
BCVN4.1		1430	72.8 ± 2.6
BCVN5'		666	21.8 ± 2.9
BCVN3'		830	65.9 ± 2.5
BCVN3' SpeI		377	11.9 ± 0.7
BCVN3'3'		497	56.6 ± 3.7
CAT		897	24.1 ± 2.3
pGEM		1818	16.3 ± 6.4

^a Mean percentage RNA bound ± SD of three filter-binding experiments for each RNA.

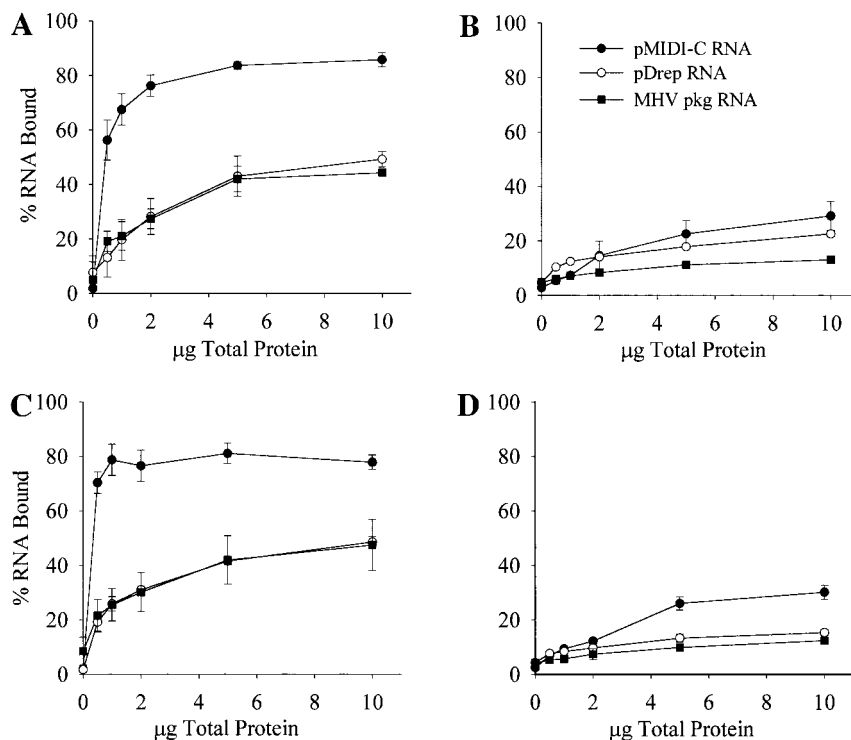


FIG. 8. Nitrocellulose filter binding of proteins from BCV- and MHV-infected lysates to BCV and MHV RNAs. Different amounts of BCV-infected HCT lysate (A), MHV-infected 17C11 lysate (C), mock-infected HCT lysate (B), or 17C11 lysate (D) were incubated with labeled BCV- and MHV-defective genome RNAs and a transcript containing the MHV packaging signal. Each data point represents the average of three experiments. The error bars depict the standard deviation of the means.

served for all RNAs using mock-infected lysates (data not shown). Taken all together, the data indicated that a high-efficiency N-binding sequence is located within the 3' terminal 434 nucleotides of the N ORF.

To directly demonstrate N-binding to the regions that exhibited the highest-efficiency binding, UV crosslinking and Western blotting were performed on filter-binding reactions. N bound the high-efficiency binding transcript N3'3' that mapped at the 3' end of the N ORF (Fig. 7A, lanes 8 and 9). However, N was not crosslinked to the Drep fragment N3' *SpeI* that was retained on filters comparably to the noncoronavirus RNAs (Fig. 7A, lanes 6 and 7), thus directly demonstrating that N accounts for the increased binding observed over the background binding of cellular proteins.

We recently showed that a region of the BCV genome shares homology with the packaging signal of MHV and demonstrated that it is a functional packaging signal (Cologna and Hogue, 2000). Even though Drep does not contain this region of the genome, we also measured N-binding to this RNA to compare it with the binding data for Drep. About 37% of the BCV pkg transcripts were bound by N, indicating that N interacts with the packaging signal, but interestingly, not as efficiently as with a region of the N ORF. UV crosslinking and Western blotting confirmed that N bound the packaging signal-containing transcript (Fig. 7A, lanes 4 and 5).

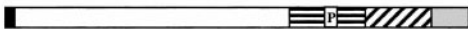
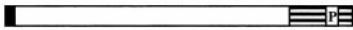

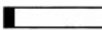


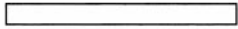
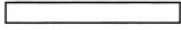
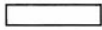







Both MHV-A59 N and BCV N bind MIDI-C at a higher efficiency than does Drep

As we mapped the N-binding regions within Drep, we wanted to determine how the high-efficiency binding region within the N ORF compared with efficiency of N-binding to the MHV packaging signal. The MHV DI genome MIDI-C was used for this analysis. At the time these measurements were made, we had not identified the BCV genomic packaging signal. The rationale for our interest in comparing N-binding to MHV and BCV RNAs was discussed earlier. MIDI-C contains a known packaging signal, and MHV and BCV are closely related, but distinct viruses.

Initially we used mock-infected and both BCV- and MHV-A59-infected cell lysates to compare the RNA-binding efficiencies of MIDI-C, Drep, and the MHV packaging signal (Fig. 8). BCV- and MHV-infected lysates were compared to rule out the possibility that differences in the N proteins from the respective viruses might affect N-RNA interactions (Figs. 8A and 8B, respectively). The binding efficiencies for the RNA transcripts were essentially the same for both lysates. The binding efficiencies for all RNAs were much lower when mock-infected lysates from either HCT (Fig. 8B) or 17C11 (Fig. 8D) cells were used. The results demonstrated that N interacts with Drep similar to the interactions of N with the MHV pack-

TABLE 2

Maximum MHV N Binding Efficiencies for MIDI-CC and Related RNAs

Transcript	Schematic	Size (nt)	Maximum N binding efficiency ^a
MIDI-C		~5500	86.0 ± 2.6
MIDI-C <i>Mlu</i> I		4435	81.6 ± 3.8
MIDI-C <i>Spe</i> I		3689	89.0 ± 2.8
MIDI-C <i>Eco</i> RI		1314	54.9 ± 4.7
MIDI-C <i>Bam</i> HI		461	26.2 ± 4.0
MHV leader		181	26.2 ± 3.4
MHV5' <i>Sal</i> I		3258	80.8 ± 4.8
MHV5' <i>Nsp</i> V		2379	74.8 ± 4.1
MHV5' <i>Hind</i> III		1553	72.1 ± 2.2
MHV5' <i>Afl</i> II		492	7.9 ± 2.0
MHV pkg		594	48.6 ± 2.0
MHV N		1413	49.6 ± 2.8
MHV N 5'		654	13.7 ± 0.9
MHV NΔ5'3'		444	13.7 ± 2.3
MHV N3'		385	55.4 ± 3.7
pGEM		1818	26.4 ± 3.5

^a Mean percentage RNA bound ± SD of three filter-binding experiments for each RNA.

aging signal. The higher level of MIDI-C retention strongly suggested that N might bind other sites in addition to the 69-nt packaging signal within the RNA.

We confirmed that MHV N protein was associated with the majority of the MIDI-C RNA retained by direct filter binding as described above for BCV. Approximately 60% of MIDI-C RNA was retained by direct filter binding in the presence of MHV-infected cell lysates. About 40% of the retained protein-RNA complexes were recovered by immunoprecipitation, thus indicating that at least 67% of the MIDI-C RNA was associated with N (Fig. 6B). Only background levels of RNA were recovered by immunoprecipitation when infected lysates were used as the source of protein or when the control pGem RNA was incubated with either lysate (Fig. 6B).

The MHV packaging signal is not required for high-efficiency binding of MIDI-C

The difference in binding efficiencies between MIDI-C and its packaging signal led us to extend our mapping analysis of the DI. Maximum binding efficiencies were measured for a series of MIDI-C-deletion transcripts using MHV-infected cell lysates (Table 2). Binding efficiencies for 3' terminal deletions MIDI-C *Mlu*I and MIDI-C *Spe*I were comparable to the binding efficiency for intact MIDI-C RNA. Interestingly, the MIDI-C *Spe*I transcript lacked the MHV packaging signal. A shorter transcript, MIDI-C *Eco*RI, from approximately 1.3 kb of the

5' end of MIDI-C, exhibited a significantly lower maximum N-binding efficiency when compared to that of full-length MIDI-C. The binding for the ~1.3-kb transcript was similar to measurements for MHV pkg, the RNA transcript containing the packaging signal. We also included a transcript of the MHV N ORF in our mapping analysis since we had identified the high-efficiency binding site within the BCV N ORF, as described above. The MHV N transcript had a binding efficiency similar to the MHV pkg RNA. Binding, like that for BCV, mapped to the 3'-most region of the MHV N ORF.

To further map the binding region within the polymerase 1a region, a fragment (nts 461–3689) of MIDI-C was subcloned and used to generate four transcripts that encompassed this region. The MHV5' *Sal*I transcript bound N as efficiently as MIDI-C RNA. Shorter transcripts, MHV5' *Nsp*V and MHV5' *Hind*III, exhibited slightly reduced levels of N-binding, compared to those of MIDI-C. Binding was greatly reduced for MHV5' *Afl*II 492-nt transcript. This indicated that a high-efficiency binding site maps between the *Afl*II and *Hind*III sites (nts 935–1986).

N-binding to full-length MIDI-C, the 5' *Hind*III region from gene 1a, the MHV packaging signal and the 3' end of the N ORF was demonstrated directly by UV crosslinking and Western blotting as described earlier (Fig. 7B, lanes 4–9 and 12 and 13). No N binding was detected with the N 5'3' ~400-nt transcript from the N

ORF in MIDI-C that exhibited only background binding when analyzed by filter binding (Fig. 7B, lanes 10 and 11).

Collectively, the mapping data for MIDI-C demonstrate that at least three N binding sequences are located in MIDI-C. One maps to a region that includes the packaging signal (nts 3949–4524), a second signal is located in the N ORF (nts 4837–5197), and another within an approximately 1-kb region of the polymerase 1a region (nts 935–1986).

The high-efficiency N-binding region within the BCV N ORF does not function as a packaging signal

The presence of a single high-efficiency binding site within the BCV N ORF was consistent with our initial hypothesis that a packaging signal located within the gene might account for packaging of Drep, and possibly subgenomic RNAs in BCV virions. To test this hypothesis, experiments were performed as we recently described for the identification of a BCV packaging signal (Cologna and Hogue, 2000). The 3' N gene region was subcloned 5' to the chloramphenicol acetyltransferase (CAT) gene that contained the hepatitis delta virus ribozyme and T7 terminator at its 3' end. The BCV packaging signal appended at the 5' end of the CAT-ribozyme-T7 terminator cassette and CAT-ribozyme-T7 terminator construct were used as positive and negative controls, respectively (Cologna and Hogue, 2000). In addition the CAT-ribozyme-terminator cassette was subcloned downstream of full-length Drep to generate pDrepE-CAT.R.

All plasmid constructs were expressed in BHK cells using the vaccinia recombinant vTF7-3 (Fuerst *et al.*, 1986), followed by infection with BCV as we described previously (Cologna and Hogue, 2000). Extracellular BCV virions were collected at 24 h after infection with BCV. Both intracellular and RNase-treated, purified virion RNA were analyzed by Northern blotting with a probe specific for Drep. The results demonstrated that the 3' region of the N ORF RNA was not sufficient to target CAT for packaging extracellular BCV virions (Fig. 9, lanes 6 and 16). Surprisingly, the entire Drep RNA also did not target CAT for packaging (Fig. 9, lanes 5 and 15). Implications of these observations are discussed below.

DISCUSSION

This study demonstrates for the first time that N interacts with both genomic and subgenomic RNAs in BCV-infected cells. N–viral RNA complexes were previously shown to be present in cells infected with MHV, a virus that is closely related to BCV (Baric *et al.*, 1988). Since the viral leader is common to genomic and subgenomic RNAs, the earlier study suggested that interactions between the leader and N could explain the presence of these complexes in virus-infected cells (Baric *et al.*, 1988). N-binding to coronavirus leader RNA supports this

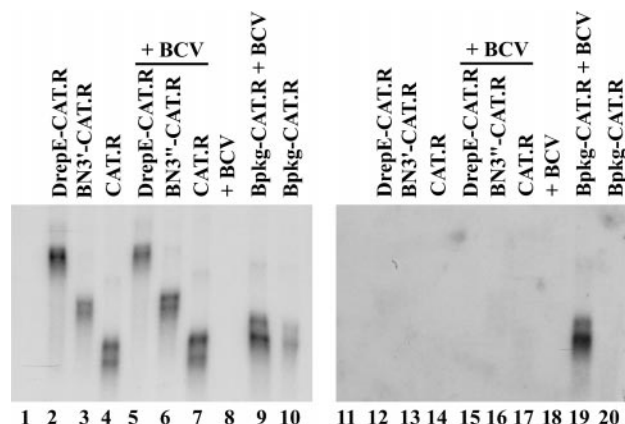


FIG. 9. Northern blot analysis of chimeric RNA transcripts packaged by BCV. Plasmid DNAs (lanes 2–7, 9 and 10, 12–17, and 19 and 20) were transfected into vTF7-3-infected cells (all lanes). +BCV denotes cells that were infected with BCV following transfection (lanes 5–9 and 15–19). Both intracellular RNAs (lanes 1–10) and extracellular virion RNAs (lanes 11–20) were analyzed by Northern blotting with a CAT-specific probe. Extracellular media were treated with DNase and RNase prior to isolation of virions. Cells were infected only with vTF7-3 and mock-transfected in lanes 1 and 11.

idea (Stohlman *et al.*, 1988). Recent biochemical analysis measured a dissociation constant (K_d) of 14 nM for bacterially expressed MHV N-binding to the leader RNA (Nelson *et al.*, 2000). We also found that N interacts *in vitro* with both BCV and MHV leader RNAs in the presence of excess nonspecific competitor RNA. Complexes consisting of N and small leader-containing RNAs are present in MHV-infected cells (Baric *et al.*, 1988). We have also immunoprecipitated small (>100 nt) N–leader containing RNA complexes from BCV-infected cells (Cologna and Hogue, unpublished data).

Taken all together the results from these studies suggest that N–RNA complexes are conserved structures in coronavirus-infected cells. Conservation of such complexes argues in support of the idea that N–RNA interactions play important roles in viral transcription, translation, and/or replication (Nelson *et al.*, 2000). Our results suggest that interactions between N and the N ORF, a region that is also common to all of the viral RNAs, may contribute, in addition to interactions with the leader, to the formation of the N–RNA complexes that are present in coronavirus-infected cells. Previous studies suggested that N binds nonspecifically to RNA. (Robbins *et al.*, 1986; Masters, 1992). Our data clearly demonstrate that N binds noncoronavirus and coronavirus RNAs both *in vivo* and *in vitro*; however, the protein interacts more efficiently with the latter.

A major goal when we initiated this study was to identify the signal(s) responsible for packaging of the BCV-defective genome Drep. We were particularly interested in this since the defective genome lacks the packaging signal that we subsequently identified within the BCV genome and because BCV packages subgenomic

RNAs in addition to genomic RNA (Hofmann *et al.*, 1990; Chang *et al.*, 1994; Cologna and Hogue, 2000). We mapped one high-efficiency N-binding region in the 3' half of the N ORF within Drep RNA. However, a nonviral RNA that contained the N-binding region was not packaged, suggesting that interactions between N and this region of the RNA do not explain why Drep or subgenomics are packaged by BCV. Even though the high-efficiency binding region does not appear to be directly relevant for packaging, interactions between N and this region of the genome may play a role indirectly in the assembly of the helical nucleocapsid. Interestingly we also mapped a high-efficiency N-binding site within the 3' half of the MHV N ORF. N presumably binds multiple regions throughout the genomic RNA. High-efficiency N-binding sites, other than the packaging signal, may contribute to the efficiency of packaging, while not being a functional packaging signal.

Surprisingly, when Drep was expressed as part of a chimeric CAT RNA transcript, the RNA was also not packaged by BCV. We cannot rule out the possibility that, if Drep contains a packaging signal, the folding of the chimeric RNA masked it. It is also possible that the defective genome must be replicated subsequent to or concurrent with packaging. Preliminary data in our lab support the idea that replication and packaging may be coupled, and experiments are ongoing to address this.

Different maximum N-binding efficiencies were measured for Drep and MIDI-C, defective genomes for BCV and MHV, respectively. We were able to calculate only rough estimates for K_d s since our his-tagged N protein preparations were not absolutely pure. Analysis of our data for N-binding to MIDI-C and Drep RNAs yielded K_d s of ~ 21 and ~ 89 nM, respectively. The K_d for N binding to noncoronavirus transcripts was ~ 1 mM. The differences in binding activity for MIDI-C and Drep may have important implications for the comparative efficiency with which the two defective genomes are encapsidated and packaged.

Packaging signals have been identified for both MHV and BCV (van der Most *et al.*, 1991; Fosmire *et al.*, 1992; Cologna and Hogue, 2000). Intuitively one might expect a packaging signal to exhibit the highest N-binding when compared to other parts of the genome. However, this is not the case for MIDI-C, at least under the *in vitro* conditions used in our study. N bound as efficiently to MIDI-C RNA when the packaging signal was deleted as it did to MIDI-C that contained the packaging signal. Molenkamp and Spaan (1997) initially showed that N binds the MHV packaging signal, but binding affinities were not measured and N-binding sites were not mapped for other regions of MIDI-C. We measured a K_d of ~ 100 nM for N-binding to an ~ 600 -nt transcript that included the MHV packaging signal. At this time it is not clear what distinguishes other N-binding sites within the genome from N-binding to the packaging signal. Under

the *in vitro* assay conditions used here it appears that binding efficiency might not be the determining factor. However, the context within which the signal is presented within the genome may alter the interactions, even though the packaging signal alone is sufficient to direct an RNA to be packaged in either MHV- or BCV-infected cells (Bos *et al.*, 1997; Woo *et al.*, 1997; Cologna and Hogue, 2000).

The packaging signal by itself may not determine the efficiency of genomic RNA packaging. Bos and colleagues (1997) inserted an intergenic sequence into MHV MIDI-C to direct the synthesis of a subgenomic RNA containing the MHV packaging signal; the subgenomic was packaged less efficiently than the parental MIDI genomic RNA. This suggests that other factors may be involved in determining the efficiency of packaging. These elements could be a specific sequence(s) or structure(s) that functions as a packaging enhancer by binding N and allowing the RNA to be more efficiently encapsidated and packaged into mature virions. The element(s) within gene 1a that we identified are possibly important in this regard. We are currently testing this possibility. Sequences that enhance packaging have been identified for other viruses. For example, naturally occurring Sindbis virus DI RNAs contain a sequence at the 5' end that enhances packaging (Frolova *et al.*, 1997).

Our data suggest that both monomeric and oligomeric forms of N interact with RNA. These interactions may be important for the assembly of the encapsidated RNA, since it is logical to think that N-N interactions occur in the helical nucleocapsid. Trimeric forms of N associated with both MHV and BCV virions were previously noted (Hogue *et al.*, 1984; Robbins *et al.*, 1986). *In vitro* interactions between N monomers were recently reported (Wang and Zhang, 1999), which is consistent with the ability of N to form multimers associated with RNA. Our data are the first to directly show that oligomers of N bind RNA.

Packaging signals have been identified for a number of viruses, and NC-RNA interactions have been studied for some of these. The Sindbis capsid protein specifically binds with high affinity to a 132-nt region within the viral RNA genome that is a functional packaging signal (Weiss *et al.*, 1994). The NC protein of human immunodeficiency virus type 1 (HIV-1) binds specifically to several stem loops near the 5' end of the genome that constitute a packaging signal. The NC has an apparent K_d of about 200 nM for the individual stem loops or 50 nM for the group of stem loops (Clever *et al.*, 2000).

Interactions between nucleocapsid proteins and RNA for other viruses with helical nucleocapsids have been studied; however, extensive mapping as we describe here has not been done. Influenza virus nucleoprotein NP appears to bind the viral RNA backbone without apparent sequence specificity (Yamanaka *et al.*, 1990; Baudin *et al.*, 1994). Binding affinity for segment 8 viral

RNA (vRNA), conserved 5' and 3' ends of the vRNAs, and degenerate sequences were all bound at similar affinities with K_d s that ranged from 20 to 38 nM. The affinity of vesicular stomatitis virus (VSV) N protein for leader RNA that contains the VSV encapsidation signal is ~10 times higher than that for nonspecific sequences (Blumberg *et al.*, 1983). The results presented here indicate that coronavirus N, like influenza virus NP, does not exhibit absolute specificity for only coronavirus RNAs. However, the protein does appear to preferentially bind coronavirus RNAs. Furthermore, N binds certain regions of the viral RNAs better than others. Binding specificity for encapsidation and packaging in the context of virus-infected cells may be influenced by interactions with the membrane (M) protein or possibly other viral proteins. Compartmentalization of replication complexes in membranous structures may also provide an environment that eliminates the necessity for absolute N-binding specificity.

MATERIALS AND METHODS

Viruses and cell lines

The human adenocarcinoma ileocecal cell line HCT-8 was maintained in Dulbecco's modified Eagle's medium (DMEM). Baby hamster kidney (BHK-21) cells were grown in Glasgow minimal essential medium (GMEM). Both cell lines were obtained from ATCC (Rockville, MD). Mouse 17 clone 1 (17Cl1) cells were propagated in DMEM. All media were supplemented with 10% fetal bovine serum (FBS). Plaque-purified bovine enteric coronavirus (BCV) Mebus strain virus stock was grown and titered on HCT-8 cells as previously described (Nguyen and Hogue, 1997). The MHV-A59 virus strain was grown on 17Cl1 cells and titered on 17Cl1 and DBT cells. The vTF7-3 recombinant vaccinia virus expressing T7 RNA polymerase (Fuerst *et al.*, 1986) virus stock was grown on HeLa cells and titered on CV-1 and BS-C-1 cells.

Plasmids

Coronavirus-defective genomes, pDrep (Chang *et al.*, 1994), and pMIDI-C (van der Most *et al.*, 1991) were obtained from David Brian (University of Tennessee-Knoxville) and Willy Spaan (Leiden University, The Netherlands), respectively. Convenient restriction sites, PCR amplification, and standard methods for DNA manipulation were used to generate fragments of the defective genomes (Fig. 1, Tables 1 and 2). All fragments were subcloned into pGEM-3Zf(+) (Promega, Madison, WI). All PCR products were confirmed by sequencing.

All N fragments were generated from plasmid pBCVN4.1. Plasmid pBCVN4.1 contains the entire N gene derived from the original MA7 cDNA genomic clone (Lapps *et al.*, 1987). The clone contains 8 nts 5' to the start codon and 24 nts following the stop codon. Plasmid

pPol was created by PCR amplification of nucleotides 98 to 472 from the polymerase region of pDrep. *Bam*HI and *Eco*RI sites were included in the PCR product at the 5' and 3' ends of the coding sequence, respectively. Plasmid pBCVN5' was created by subcloning the *Eco*RI/*Bgl*II fragment from pBCVN4.1 into *Eco*RI/*Bam*HI restricted vector. The *Bgl*II/*Hind*III fragment of pBCVN4.1 was subcloned into *Bam*HI/*Hind*III cut vector to construct plasmid pBCVN3'. Plasmid pBCVN3'3' was generated by subcloning the *Spe*I/*Hind*III fragment of pBCVN3' into *Xba*I/*Hind*III cut vector. Plasmid pBCVpkg was previously described (Cologna and Hogue, 2000). The 5' end of the BCV gene 1a was subcloned from Drep by PCR amplification. Construction of pBCV3'NCR was previously described (Spagnolo and Hogue, 2000). Plasmid pBCVN4 contains the entire N gene as described above for pBCVN4.1 that was modified to contain a hepatitis delta ribozyme and T7 terminator. This was accomplished by subcloning a fragment that contains both elements from plasmid v2.0 (Pattnaik *et al.*, 1992) at the 3' end of the N ORF.

Plasmid DrepE-CAT.R was generated by introduction of an *Eco*RI site at the 5' end of Drep and subcloning of a cassette that contained the CAT gene, the hepatitis delta virus ribozyme, and the T7 terminator at the 3' end. The other chimeric constructs (BN3'-CAT.R, Bpkg-CAT.R, and pGEM-CAT.R) and the CAT cassette were all previously described (Cologna and Hogue, 2000).

Plasmid pMHVpkg was constructed by PCR amplification of a fragment encompassing nucleotides 3941 to 4529 from pMIDI-C. The PCR strategy introduced an *Eco*RI site at the 5' end of the coding sequence and a *Bam*HI site at the 3' end for subcloning purposes. Plasmid pMHVN1 that includes the entire MHV A59 N gene, plus 6 nt 5' to the start codon and 16 nt from the 3' noncoding region sequences, was PCR-amplified from plasmid pA50 (Masters, 1992). *Kpn*I and *Xba*I sites were introduced during amplification at the 5' and 3' ends of the MHV N coding sequence, respectively. Plasmid pMHV N5' was generated by subcloning the 5' *Eco*RI/*Nhe*I fragment from pMHVN and subcloning into *Eco*RI/*Xba*I cut vector. The internal *Nhe*I/*Eco*RI 405 nt fragment from pMHVN was subcloned into *Eco*RI/*Xba*I cut vector to create pMHV N Δ 5'3'. Plasmid pMHVN was restricted with *Eco*RI and the 3.5-kb fragment, which included all of the vector plus 382 nt from the 3' end of the N gene, was isolated and religated to make pMHV N3'.

Plasmid pNAR1 was generated by subcloning the *Sma*I/*Hind*III fragment from v2.0 (Pattnaik *et al.*, 1992) into *Sma*I/*Hind*III restricted pNA (Brown *et al.*, 1988).

Preparation of RNA transcripts

Convenient restriction sites were used to linearize DNAs for *in vitro* transcription of both unlabeled and [α - 32 P]CTP-labeled transcripts that were used for filter

binding. Transcripts contained 0–38 nt and 0–30 nt at the 5' and 3' termini, respectively. These exogenous nucleotides were encoded by restriction sites retained from the multiple cloning region of pGEM-3Zf(+) during subcloning. Vector pGEM-3Zf(+) (Promega) that had been cut with *ScaI* was used to generate runoff of an ~1.8-kb transcript as a noncoronavirus control. All positive-sense transcripts, with the exception of BCV pPol and pMHVN Δ 5'3' that were transcribed from the SP6 promoter, were generated from the T7 promoter. Unlabeled RNAs were transcribed using either Promega or Megascript (Ambion, Austin, TX) reagents according to the manufacturer's protocols. Unlabeled RNAs were monitored on nondenaturing agarose gels stained with ethidium bromide and quantitated by standard absorbance readings at A_{260} . DNA templates were removed by digestion with DNase following transcription. Free nucleotides were removed from labeled transcripts using micro Bio-Spin columns (Bio-Rad, Richmond, CA), which has been washed extensively with RNase-free water. RNAs were monitored on nondenaturing agarose gels stained with ethidium bromide. RNAs were quantified and specific activity was calculated using standard protocols.

Capped Drep and MIDI-C RNAs for defective genome replication and packaging studies were generated using T7 MEGAscript kit (Ambion) following the manufacturer's protocol. RNAs were precipitated following DNase treatment and quantified by absorbance at 260 nm; integrity was monitored by electrophoresis on agarose gels and ethidium bromide staining.

Generation of N-specific polyclonal antibodies

A histidine-tagged BCV N fusion protein was expressed and purified from bacteria as previously described (Cologna and Hogue, 1998). Six histidine residues replaced the first 17 amino acids at the amino-terminus of the BCV N protein. Two female New Zealand White rabbits were inoculated with the purified histidine-tagged N protein using standard protocols (Harlow, 1988). Antibodies were purified by selection over a protein A column (Bio-Rad) as recommended by the manufacturer. Western blotting and immunoprecipitations determined the specificity of the antibodies.

Detection of RNAs associated with N during a BCV infection by agarose gel electrophoresis

Subconfluent monolayers of HCT cells were infected with BCV at a multiplicity of infection (m.o.i.) of 10. After infection cells were incubated in DMEM containing 2% FBS. At 4 h postinfection (p.i.), cells were labeled with [32 P]orthophosphate (200 μ Ci/ml) for 4 h in phosphate-free DMEM containing 5% FBS that had been dialyzed. One dish of mock- and BCV-infected cells was labeled in the presence of 2 μ g/ml actinomycin D to specifically label only viral RNAs. Total cytoplasmic RNA was iso-

lated from cells at 8 h p.i. with TRIzol (Life Technologies, Gaithersburg, MD). To isolate N-associated RNAs, cells were washed with cold PBS and lysed in immunoprecipitation (IP) lysis buffer (10 mM Tris-HCl [pH 7.4], 100 mM NaCl, 20 mM EDTA, 5 mM MgCl₂, 0.5% Triton X-100, 0.5% sodium deoxycholate [DOC], 1 mM PMSF, and 10 mM iodoacetamide). Nuclei and cell debris were removed by centrifugation at 4°C for 10 min at 13,000 *g*. Lysates were immunoprecipitated with either preimmune serum, purified 1383 anti-N rabbit polyclonal antibodies, or a mix of monoclonal anti-BCV S ascites antibodies (HB10-4, JB5-6, and HF8-8) (Deregt and Babiuk, 1987). Protein A-Sepharose-bound immune complexes were washed three times in IP lysis buffer supplemented with 0.1% SDS. Protein-RNA complexes were eluted in 50 μ l of elution buffer (10 mM Tris-HCl [pH 7.4], 50 mM NaCl, 1 mM EDTA, 200 μ g/ml yeast tRNA, and 1.0% SDS). RNAs were extracted with TRIzol (Life Technologies), washed with 70% ethanol, and air-dried. Standard conditions for denaturing and electrophoreses on 1% agarose gels containing 2.2 M formaldehyde were followed. The gels were washed extensively with RNase-free water, dried, and autoradiographed.

Isolation of N-RNA complexes formed during vaccinia expression and Northern blot analysis

Subconfluent BHK-21 cells were infected with vTF7-3 (Fuerst *et al.*, 1986) at a m.o.i. = 10 for 1 h in GMEM and transfected essentially as previously described (Nguyen and Hogue, 1997). Following infection, cells were transfected with a total of 15 μ g of pNA.R1 or pBCVN4.1 DNA using 15 μ l of Lipofectin (Life Technologies). Cells were harvested 16 h p.i. in IP lysis buffer as described above. The lysates were divided into three aliquots. One aliquot was extracted for total RNA and the other two aliquots were immunoprecipitated with either purified 1383 anti-N rabbit antibodies or anti-NA peptide polyclonal serum (Hogue and Nayak, 1992). Total RNA samples were treated with RQ1-RNase-free DNase. N-RNA and NA-RNA complexes were immunoprecipitated as described above. RNAs were denatured, electrophoresed on a 1% agarose gel in the presence 2.2 M formaldehyde, transferred to NitroBind membrane (Amersham Pharmacia Biotech, Piscataway, NJ) by vacuum transfer, and probed with either a BCV N gene-specific or an influenza NA gene-specific riboprobe uniformly labeled with [α - 32 P]CTP.

In-solution binding assay

The in-solution binding assay was carried out essentially as described previously (Geigenmuller-Gnirke *et al.*, 1993). *In vitro* transcribed, nonlabeled RNAs were incubated with *in vitro* translated [35 S]methionine-labeled N protein in a binding buffer that consisted of 10 mM Tris-HCl (pH 7.4), 100 mM NaCl, 1 mM EDTA, 1 unit

RNasin, and 5 μg of BHK total cytoplasmic RNA. Total reaction volume was 10 μl . The amount of translated N included in each reaction varied from 0.2 to 5 μl and was determined by the extent of incorporation of [^{35}S]methionine during translation. Reactions were incubated for 20 min at room temperature and 2 μl of dye (20% Ficoll, 0.05% bromophenol blue in 0.25 \times TBE) was added to each reaction before loading on a 1% nondenaturing agarose gel in 0.25 \times TBE. Gels were electrophoresed at 30 mA for 4 h, soaked in methanol, dried, and autoradiographed.

Preparation of cell lysates

HCT cells were infected with BCV at a m.o.i. of 5 and harvested at 16 h after infection. MHV-A59-infected 17C11 cells were harvested 12 h p.i. Mock-infected cells were maintained and prepared in parallel. Cells were harvested by washing twice with ice-cold PBS and washing briefly with 1 \times hypotonic buffer containing 10 mM Tris-HCl (pH 7.4), 10 mM NaCl, 1 mM PMSF, 10 mM iodoacetamide, and 1 \times proteinase-inhibitor cocktail minus EDTA (Boehringer Mannheim, Indianapolis, IN). Cells were scraped into 0.5 \times hypotonic buffer and incubated on ice for 10 min before Dounce homogenization. Aliquots of the lysates were stored at -80°C . Protein concentrations were determined for each lysate using the BCA Protein Assay (Pierce, Rockford, IL). Cytoplasmic lysates were stable for about 1 month.

Filter-binding assay

Filter-binding reactions were carried out in a volume of 20 μl . Reaction buffer consisted of 10 mM Tris-HCl (pH 7.4), 1 mM DTT, 1 mM EDTA, 250 mM NaCl, 1 unit RNasin, 5.0 μg BHK total cytoplasmic RNA, and 10 μg heparin. Cytoplasmic lysates or purified proteins (0.5–10 μg) were incubated with 0.1 nM of labeled RNA for 20 min at room temperature. Reaction mixtures were filtered through prewetted 0.45- μm -pore-size nitrocellulose filters, washed twice with ice-cold wash buffer (10 mM Tris-HCl [pH 7.4], 100 mM NaCl, and 1 mM EDTA) and air-dried. Only RNA complexed with protein was retained on the filters and was detected by Cerenkov counting. The total amount of radioactivity added to each reaction was determined by spotting 0.1 nM of labeled RNA probe onto nitrocellulose filters and Cerenkov counting. The percentage of RNA retained on filters was calculated using the following formula: %RNA = (cpm retained on filter per reaction/total cpm added to the reaction) \times 100.

UV crosslinking/Western blotting

Filter-binding reactions were assembled as described above. After incubation reactions were placed on ice and UV-irradiated at 254 nm (UV Stratallinker; Stratagene, La Jolla, CA) at a distance of 10.5 cm for 30 min. After crosslinking, 1 μg RNase A and 10 units RNase T₁ were

added to each reaction. Reactions were incubated for 15 min at 37°C . SDS-PAGE sample buffer was added to the reactions. Samples were heated at 95°C before being resolved by SDS-PAGE. Following electrophoresis gels were electroblotted to nitrocellulose membranes. Western blots were probed with rabbit anti-N antibodies, followed by goat anti-rabbit secondary IgG conjugated to alkaline phosphatase.

N-RNA complex immunoprecipitation

For immunoprecipitation of N-RNA complexes, filter-binding reactions were assembled as described above. After incubation half of each reaction was analyzed directly for retention of RNA on filters. The other half of each reaction was incubated with purified N-specific antibodies (rabbit 1383) for 30 min on ice, followed by incubation with protein A-Sepharose for 1 h. Immunoprecipitates were washed three times with filter-binding wash buffer. N-RNA complexes bound to protein A-Sepharose were analyzed by Cerenkov counting. The percentage of RNA immunoprecipitated was calculated using the formula: %RNA IP = (cpm bound to protein A-Sepharose/half of the cpm added to binding reaction) \times 100.

ACKNOWLEDGMENTS

This work was supported by Public Health Service Grant AI33500 to B.G.H. from the National Institute of Allergy and Infectious Diseases. R.C. and J.F.S. were supported in part by NIH Training Grant T32AI07471.

REFERENCES

- Abraham, S., Kienzle, T. E., Lapps, W., and Brian, D. A. (1990a). Deduced sequence of the bovine coronavirus spike protein and identification of the internal proteolytic cleavage site. *Virology* **176**, 296–301.
- Abraham, S., Kienzle, T. E., Lapps, W. E., and Brian, D. A. (1990b). Sequence and expression analysis of potential nonstructural proteins of 4.9, 4.8, 12.7, and 9.5 kDa encoded between the spike and membrane protein genes of the bovine coronavirus. *Virology* **177**, 488–495.
- Baric, R. S., Nelson, G. W., Fleming, J. O., Deans, R. J., Keck, J. G., Casteel, N., and Stohlman, S. A. (1988). Interactions between coronavirus nucleocapsid protein and viral RNAs: Implications for viral transcription. *J. Virol.* **62**, 4280–4287.
- Baudin, F., Bach, C., Cusack, S., and Ruigrok, R. W. (1994). Structure of influenza virus RNP. I. Influenza virus nucleoprotein melts secondary structure in panhandle RNA and exposes the bases to the solvent. *EMBO J.* **13**, 3158–3165.
- Blumberg, B. M., Giorgi, C., and Kolakofsky, D. (1983). N protein of vesicular stomatitis virus selectively encapsidates leader RNA in vitro. *Cell* **32**, 559–567.
- Bos, E. C., Dobbe, J. C., Luytjes, W., and Spaan, W. J. (1997). A sub-genomic mRNA transcript of the coronavirus mouse hepatitis virus strain A59 defective interfering (DI) RNA is packaged when it contains the DI packaging signal. *J. Virol.* **71**, 5684–5687.
- Brown, D. J., Hogue, B. G., and Nayak, D. P. (1988). Redundancy of signal and anchor functions in the NH₂-terminal uncharged region of influenza virus neuraminidase, a class II membrane glycoprotein. *J. Virol.* **62**, 3824–3831.
- Caul, E. O., Ashley, C. R., Ferguson, M., and Egglestone, S. I. (1979).

- Preliminary studies on the isolation of coronavirus 229E nucleocapsids. *FEMS Microbiol. Lett.* **5**, 101–105.
- Chang, R. Y., and Brian, D. A. (1996). cis Requirement for N-specific protein sequence in bovine coronavirus defective interfering RNA replication. *J. Virol.* **70**, 2201–2207.
- Chang, R. Y., Hofmann, M. A., Sethna, P. B., and Brian, D. A. (1994). A cis-acting function for the coronavirus leader in defective interfering RNA replication. *J. Virol.* **68**, 8223–8231.
- Clever, J. L., Taplitz, R. A., Lochrie, M. A., Polisky, B., and Parslow, T. G. (2000). A heterologous, high-affinity RNA ligand for human immunodeficiency virus Gag protein has RNA packaging activity. *J. Virol.* **74**, 541–546.
- Cologna, R., and Hogue, B. G. (1998). Coronavirus nucleocapsid protein–RNA interactions. *Adv. Exp. Med. Biol.* **440**, 355–359.
- Cologna, R., and Hogue, B. G. (2000). Identification of a bovine coronavirus packaging signal. *J. Virol.* **74**, 580–583.
- Compton, S. R., Rogers, D. B., Holmes, K. V., Fertsch, D., Remenick, J., and McGowan, J. J. (1987). In vitro replication of mouse hepatitis virus strain A59. *J. Virol.* **61**, 1814–1820.
- Davies, H. A., Dourmashkin, R. R., and Macnaughton, M. R. (1981). Ribonucleoprotein of avian infectious bronchitis virus. *J. Gen. Virol.* **53**, 67–74.
- de Groot, R. J., van der Most, R. G., and Spaan, W. J. (1992). The fitness of defective interfering murine coronavirus DI-a and its derivatives is decreased by nonsense and frameshift mutations. *J. Virol.* **66**, 5898–5905.
- Denison, M. R., Spaan, W. J., van der Meer, Y., Gibson, C. A., Sims, A. C., Prentice, E., and Lu, X. T. (1999). The putative helicase of the coronavirus mouse hepatitis virus is processed from the replicase gene polyprotein and localizes in complexes that are active in viral RNA synthesis. *J. Virol.* **73**, 6862–6871.
- Deregt, D., and Babiuk, L. A. (1987). Monoclonal antibodies to bovine coronavirus: Characteristics and topographical mapping of neutralizing epitopes on the E2 and E3 glycoproteins. *Virology* **161**, 410–420.
- Fosmire, J. A., Hwang, K., and Makino, S. (1992). Identification and characterization of a coronavirus packaging signal. *J. Virol.* **66**, 3522–3530.
- Frolova, E., Frolov, I., and Schlesinger, S. (1997). Packaging signals in alphaviruses. *J. Virol.* **71**, 248–258.
- Fuerst, T. R., Niles, E. G., Studier, F. W., and Moss, B. (1986). Eukaryotic transient-expression system based on recombinant vaccinia virus that synthesizes bacteriophage T7 RNA polymerase. *Proc. Natl. Acad. Sci. USA* **83**, 8122–8126.
- Geigenmuller-Gnirke, U., Nitschko, H., and Schlesinger, S. (1993). Deletion analysis of the capsid protein of Sindbis virus: Identification of the RNA binding region. *J. Virol.* **67**, 1620–1626.
- Harlow, E. a. D. L. (1988). "Antibodies: A Laboratory Manual." Cold Spring Harbor Laboratory Press, Cold Spring Harbor, NY.
- Hofmann, M. A., Sethna, P. B., and Brian, D. A. (1990). Bovine coronavirus mRNA replication continues throughout persistent infection in cell culture. *J. Virol.* **64**, 4108–4114.
- Hogue, B. G., King, B., and Brian, D. A. (1984). Antigenic relationships among proteins of bovine coronavirus, human respiratory coronavirus OC43, and mouse hepatitis coronavirus A59. *J. Virol.* **51**, 384–388.
- Hogue, B. G., and Nayak, D. P. (1992). Synthesis and processing of the influenza virus neuraminidase, a type II transmembrane glycoprotein. *Virology* **188**, 510–517.
- Kennedy, D. A., and Johnson-Lussenburg, C. M. (1975). Isolation and morphology of the internal component of human coronavirus, strain 229E. *Intervirology* **6**, 197–206.
- Kienzle, T. E., Abraham, S., Hogue, B. G., and Brian, D. A. (1990). Structure and orientation of expressed bovine coronavirus hemagglutinin-esterase protein. *J. Virol.* **64**, 1834–1838.
- Lapps, W., Hogue, B. G., and Brian, D. A. (1987). Sequence analysis of the bovine coronavirus nucleocapsid and matrix protein genes. *Virology* **157**, 47–57.
- Li, H. P., Zhang, X., Duncan, R., Comai, L., and Lai, M. M. (1997). Heterogeneous nuclear ribonucleoprotein A1 binds to the transcription-regulatory region of mouse hepatitis virus RNA. *Proc. Natl. Acad. Sci. USA* **94**, 9544–9549.
- Macneughton, M. R., and Davies, H. A. (1978). Ribonucleoprotein-like structures from coronavirus particles. *J. Gen. Virol.* **39**, 545–549.
- Masters, P. S. (1992). Localization of an RNA-binding domain in the nucleocapsid protein of the coronavirus mouse hepatitis virus. *Arch. Virol.* **125**, 141–160.
- Molenkamp, R., and Spaan, W. J. (1997). Identification of a specific interaction between the coronavirus mouse hepatitis virus A59 nucleocapsid protein and packaging signal. *Virology* **239**, 78–86.
- Nelson, G. W., and Stohlman, S. A. (1993). Localization of the RNA-binding domain of mouse hepatitis virus nucleocapsid protein. *J. Gen. Virol.* **74**, 1975–1979.
- Nelson, G. W., Stohlman, S. A., and Tahara, S. M. (2000). High affinity interaction between nucleocapsid protein and leader/intergenic sequence of mouse hepatitis virus RNA. *J. Gen. Virol.* **81**, 181–188.
- Nguyen, V. P., and Hogue, B. G. (1997). Protein interactions during coronavirus assembly. *J. Virol.* **71**, 9278–9284.
- Parker, M. M., and Masters, P. S. (1990). Sequence comparison of the N genes of five strains of the coronavirus mouse hepatitis virus suggests a three domain structure for the nucleocapsid protein. *Virology* **179**, 463–468.
- Pattnaik, A. K., Ball, L. A., LeGrone, A. W., and Wertz, G. W. (1992). Infectious defective interfering particles of VSV from transcripts of a cDNA clone. *Cell* **69**, 1011–1020.
- Risco, C., Anton, I. M., Enjuanes, L., and Carrascosa, J. L. (1996). The transmissible gastroenteritis coronavirus contains a spherical core shell consisting of M and N proteins. *J. Virol.* **70**, 4773–4777.
- Robbins, S. G., Frana, M. F., McGowan, J. J., Boyle, J. F., and Holmes, K. V. (1986). RNA-binding proteins of coronavirus MHV: Detection of monomeric and multimeric N protein with an RNA overlay-protein blot assay. *Virology* **150**, 402–410.
- Spagnolo, J. F., and Hogue, B. G. (2000). Host protein interactions with the 3' end of bovine coronavirus RNA and the requirement of the Poly(A) tail for coronavirus defective genome replication [In Process Citation]. *J. Virol.* **74**, 5053–5065.
- Stohlman, S. A., Baric, R. S., Nelson, G. N., Soe, L. H., Welter, L. M., and Deans, R. J. (1988). Specific interaction between coronavirus leader RNA and nucleocapsid protein. *J. Virol.* **62**, 4288–4295.
- Tahara, S. M., Dietlin, T. A., Bergmann, C. C., Nelson, G. W., Kyuwa, S., Anthony, R. P., and Stohlman, S. A. (1994). Coronavirus translational regulation: Leader affects mRNA efficiency. *Virology* **202**, 621–630.
- van der Meer, Y., Snijder, E. J., Dobbe, J. C., Schleich, S., Denison, M. R., Spaan, W. J., and Locker, J. K. (1999). Localization of mouse hepatitis virus nonstructural proteins and RNA synthesis indicates a role for late endosomes in viral replication. *J. Virol.* **73**, 7641–7657.
- van der Most, R. G., Bredenbeek, P. J., and Spaan, W. J. (1991). A domain at the 3' end of the polymerase gene is essential for encapsidation of coronavirus defective interfering RNAs. *J. Virol.* **65**, 3219–3226.
- Wang, Y., and Zhang, X. (1999). The nucleocapsid protein of coronavirus mouse hepatitis virus interacts with the cellular heterogeneous nuclear ribonucleoprotein A1 *in vitro* and *in vivo*. *Virology* **265**, 96–109.
- Weiss, B., Geigenmuller-Gnirke, U., and Schlesinger, S. (1994). Interactions between Sindbis virus RNAs and a 68 amino acid derivative of the viral capsid protein further defines the capsid binding site. *Nucleic Acids Res.* **22**, 780–786.
- Woo, K., Joo, M., Narayanan, K., Kim, K. H., and Makino, S. (1997). Murine coronavirus packaging signal confers packaging to nonviral RNA. *J. Virol.* **71**, 824–827.
- Yamanaka, K., Ishihama, A., and Nagata, K. (1990). Reconstitution of influenza virus RNA–nucleoprotein complexes structurally resembling native viral ribonucleoprotein cores. *J. Biol. Chem.* **265**, 11151–11155.
- Zhang, X., and Lai, M. M. (1995). Interactions between the cytoplasmic proteins and the intergenic (promoter) sequence of mouse hepatitis virus RNA: Correlation with the amounts of subgenomic mRNA transcribed. *J. Virol.* **69**, 1637–1644.